Electronic supporting information:

Unveiling the Potential of Polymer Cholesteric Liquid Crystal Interpenetrating Networks as a Label-Free Alcohol Biochemical Sensor

Bhupendra Pratap Singh and Shug-June Hwang*
Department of Electro-Optical Engineering, National United University, Miao-Li 360, Taiwan.

Corresponding author e-mail address: june@nuu.edu.tw.

KEYWORDS: Polymer cholesteric liquid crystal, interpenetrating polymer network, hydrogel, optical sensor.

Contents:

Figure S1: Chemical structures representing the materials employed in the preparation of PCLC in the experimental procedure: (a) LC756, (b) 5CB, (c) I651, and (d) LC242.

Figure S2: Chemical structures of the constituent materials employed in the preparation of the hydrogel: (a) I651, (b) Acrylic Acid (AA), and (c) TPGDA.

Figure S3: Photonic bandgap spectrum of the PCLC films at the pre-cross-linking state, the post-cross-linking state, and subsequent nonreactive mesogen (5CB) extraction at varying concentrations.

Figure S4: A graph illustrating the relationship between the wavelength ratio (λ_3/λ_2) and the weight fraction of the nonreactive mesogen $(1-\phi)$.

Figure S5: A step-by-step photographic sequence demonstrating the color transformation of a PCLC film throughout the sensor fabrication process, along with its subsequent use in alcohol detection.

Figure S6: Time-lapse transmittance spectra are shown for the central dot within the $PCLC_{IPN}$ array dot when subjected to different ethanol concentrations, time-dependent wavelength shifts of $PCLC_{IPN}$ dot upon exposure to solutions with different ethanol concentrations, and the photonic wavelength bandgap (λ_{PBG}) values of the $PCLC_{IPN}$ array dot were monitored over a series of cycles, total 50 cycles.

Figure S7: Time-lapse transmittance spectra are shown for the central dot within the $PCLC_{IPN}$

array dot when subjected to different methanol solutions.

Figure S8: Response and recovery time measurement mechanism.

- **Measurements:**

The photonic bandgap spectrum of PCLC films was measured in different states: pre-cross-linking, post-cross-linking, and after nonreactive mesogen (5CB) extraction followed by hydrogel infusion. The measurements were conducted using a fiber spectrometer (Mars HS 2000+ mini, slit 25 µm by GIE Optics Co. LTD, Taiwan). Dynamic transmission measurements, including acetone treatment, NaOH functionalization, and alcohol detection, were performed using a UV-Vis spectrometer (CH2100, Spectra Academy, K-Mac, South Korea). Attenuated total reflectance-Fourier transform infrared spectroscopy (ATR-FTIR) measurements were carried out within the 500−4000 cm^{-1} range at various stages: after crosslinking, after 5CB extraction, post-hydrogel infusion, and after functionalization. These measurements were conducted using an ATR-FTIR spectrometer (Nicolet iS50, ThermoFisher Scientific, USA). Photographs of the PCLC film and $PCLC_{IPN}$ film at different stages were captured using a Samsung Galaxy A52s smartphone camera with 64MP (F1.8, OIS).

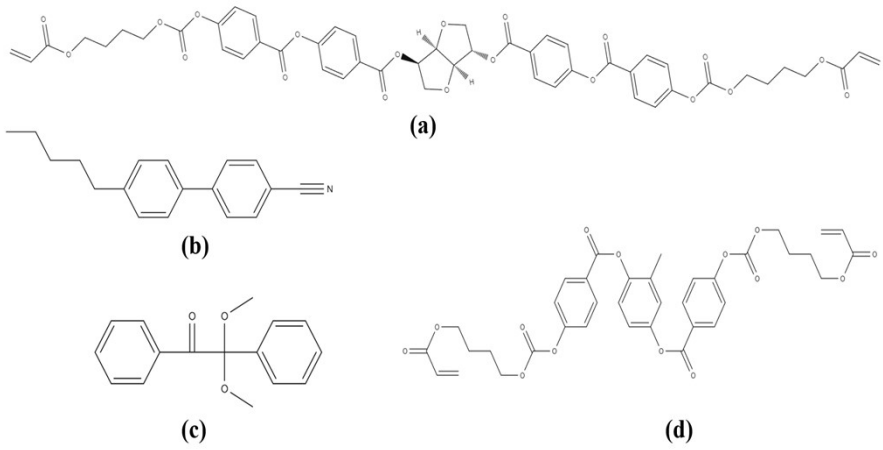

Figure S1: Chemical structures representing the materials employed in the preparation of PCLC in the experimental procedure: (a) LC756: 1,4:3,6-Dianhydro-D-glucitol bis[4-[[4 [[[4-[(1-oxo-2 propenyl)oxy]butoxy]carbonyl]oxy] benzoyl]oxy]benzoate, (b) 5CB: 4-Cyano-4'-pentylbiphenyl, (c) I651: 1,2-Diphenyl-2,2-dimethoxyethanone, and (d) LC242: 4-[[[4-[(1-Oxo-2-propenyl)oxy]butoxy]carbonyl]oxy]benzoic acid 2-methyl-1, 4-phenylene ester in ratio [LC242:69.5%, LC756:4.5%, 5CB:30% and I651:1%].

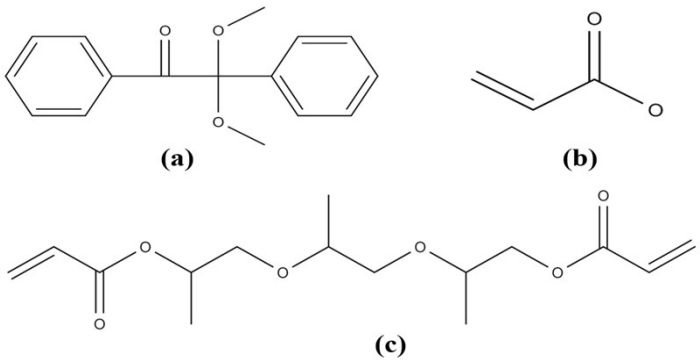

Figure S2: Chemical structures of the constituent materials employed in the preparation of the hydrogel: (a) I651: 1,2-Diphenyl-2,2-dimethoxyethanone, (b) AA: Acrylic Acid, and (c) TPGDA: Tri(propylene glycol) diacrylate in ratio [AA: TPGDA: I651=98.5:0.5:1].

- **Unlocking Insights from Photonic Structures in PCLC Films**

Initially, a comprehensive investigation was conducted on polymer cholesteric liquid crystal (PCLC) films to precisely ascertain their photonic band gap using transmission spectra analysis. Films comprising the PCLC mixture in various states, including the pre-cross-linking mixed state, the post-cross-linking state, and subsequent mesogen extraction at varying concentrations, underwent careful analysis. The wavelength corresponding to the photonic bandgap was examined through transmission spectroscopy (Fig. S3). A typical photonic bandgap spectrum has been observed for all the PCLC films under investigation. This observation suggests that the photonic PCLC structures remained intact even after the cross-linking process and the removal of the chiral dopant. Moreover, the regular periodic chiral structure of the cholesteric liquid crystal (CLC) was preserved even when substantial quantities of nonreactive mesogens (~32.5 wt%) were extracted. Subsequently, an analysis was conducted to determine the wavelength located in the middle of the bandgap. As the concentration of the nonreactive mesogen exceeds 32.5 wt%, it's important to note that the wavelength within the photonic bandgap, following the extraction of 5CB, extends beyond the range of UV-visible light.

The wavelength of the photonic bandgaps before UV cross-linking, after UV cross-linking

and after 5CB extraction can also be calculate and verified by using the equation S1 to S3 [1]:

$$\frac{\lambda_1}{n} = \frac{1}{(HTP)_1} \times \frac{1}{\phi}, \quad \text{(S1)}$$

$$\frac{\lambda_2}{\lambda_1} = \frac{n_2 p_2}{n_1 p_1} = \frac{n_2 V_2}{n_1 V_1} = \frac{n_2 W_2/\rho_2}{n_1 W_{1/\rho_1}} = \frac{n_2 \rho_1}{n_1 \rho_2}, \quad \text{(S2)}$$

and,

$$\frac{\lambda_3}{\lambda_2} = \frac{n_3 p_3}{n_2 p_2} = \frac{n_3 V_2}{n_2 V_1} = \frac{n_3 W_3/\rho_3}{n_2 W_{2/\rho_2}} = \frac{n_3 \rho_2 W_2 (1-\phi)}{n_2 \rho_3 \quad W_2} = \frac{n_3 \rho_2}{n_2 \rho_3}(1-\phi) \quad \text{(S3)}$$

where *n* is the average reflective index, ϕ is the weight fraction of the nonreactive mesogen (5CB), *HTP* is the helical twisting power, λ_1 and λ_2 is the wavelength before and after UV cross-linking of CLC mixture, *ρ* is the density, λ_3 is the wavelength at the photonic bandgap after 5CB extraction, *p* and *V* are the pitch and volume of the CLC film. The subscripts 1, 2 and 3, differentiating between states before UV crosslinking, after UV crosslinking and subsequent to nonreactive mesogen extraction, served to precisely delineate this pitch variation phenomenon.

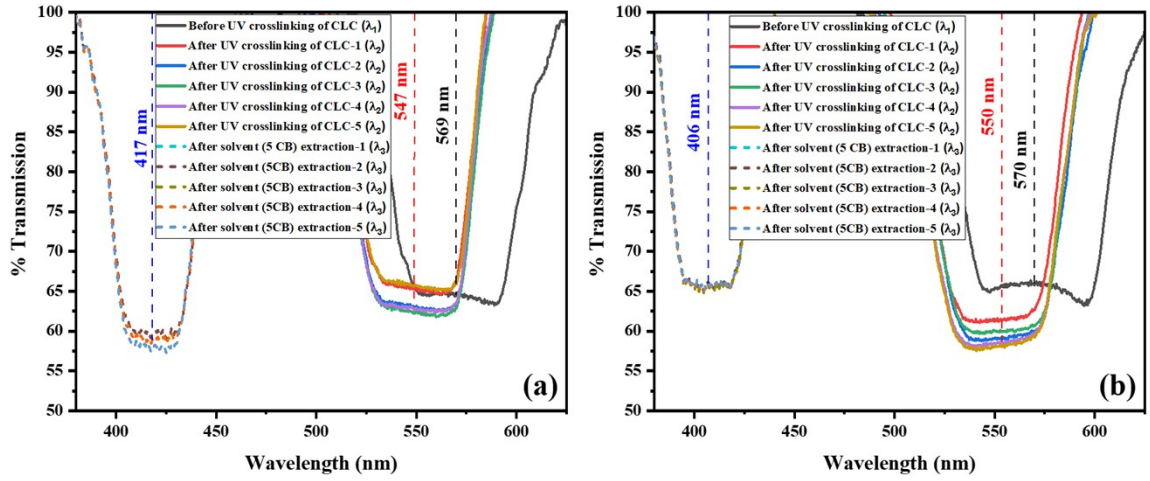

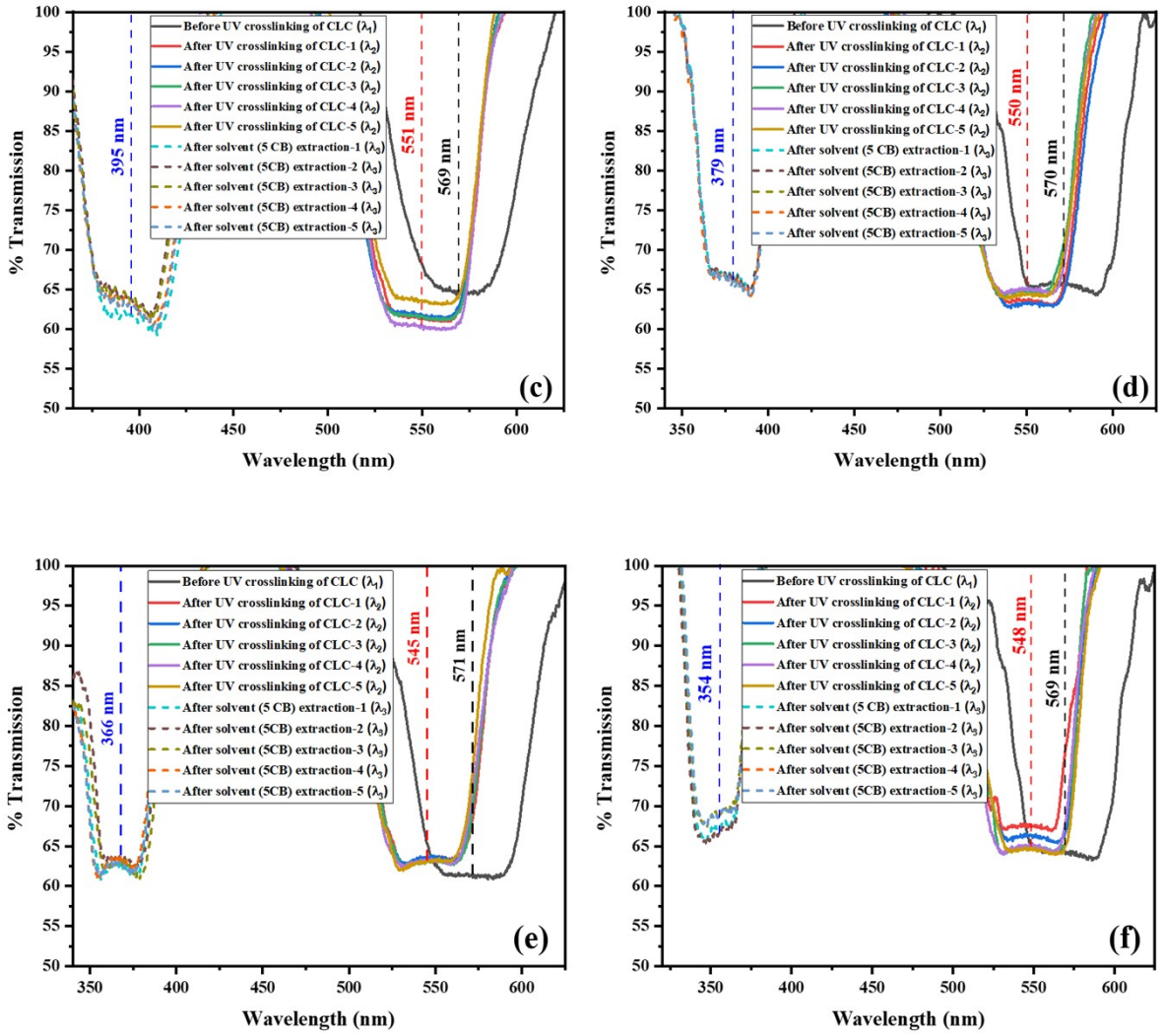

Figure S3: Photonic bandgap spectrum of the PCLC films at the pre-cross-linking state, the post-cross-linking state, and subsequent nonreactive mesogen (5CB) extraction at varying concentrations, (a) ϕ = 20%, (b) ϕ = 22.5%, (c) ϕ = 25%, (d) ϕ = 28.5%, (e) ϕ = 30%, and (f) ϕ = 32.5% (after 32.5%; It is noteworthy that the wavelength within the photonic bandgap, following the extraction of 5CB, extends beyond the range of UV-visible light).

Table S1 presented the recorded wavelengths for the globally oriented PCLC film at the photonic bandgap, both prior to UV crosslinking (λ_1), subsequent to UV cross-linking (λ_2), and subsequent to the extraction of the nonreactive mesogen (λ_3). To scrutinize the influence of UV cross-linking on the photonic structure, λ_2 was compared to λ_1, as documented in Table S1. The investigation revealed a consistent pattern across all samples, with the measured and calculated data exhibiting a substantial concurrence, resulting in a consistent λ_1/λ_2 ratio of 1.0454 ± 0.00607. The wavelength of the photonic bandgap after

solvent extraction (λ_3) had experienced a significant decrease as compared to the initial values of λ_1 and λ_2. This observed blue shift was attributed to the substantial alteration in volume resulting from the extraction of the nonreactive mesogen. The quantitative description of the pitch variation ensuing dopant extraction was expressed by Equation (S2), wherein the pitch modulation exhibited a linear correlation with the concurrent volume adjustment.

Table S1: Measured wavelengths of globally oriented PCLC film at photonic bandgap before UV cross-linking (λ_1), after UV cross-linking (λ_2) and nonreactive mesogen extraction (λ_3).

ϕ (wt%)	20	22.5	25	28.5	30	32.5
λ_1	569	570	569	570	571	569
λ_2	547	550	551	550	545	548
λ_3	417	406	395	379	366	354
λ_1/λ_2	1.0402	1.0364	1.0327	1.0364	1.0477	1.0383
λ_3/λ_2	0.7623	0.7382	0.7169	0.6891	0.6716	0.6460

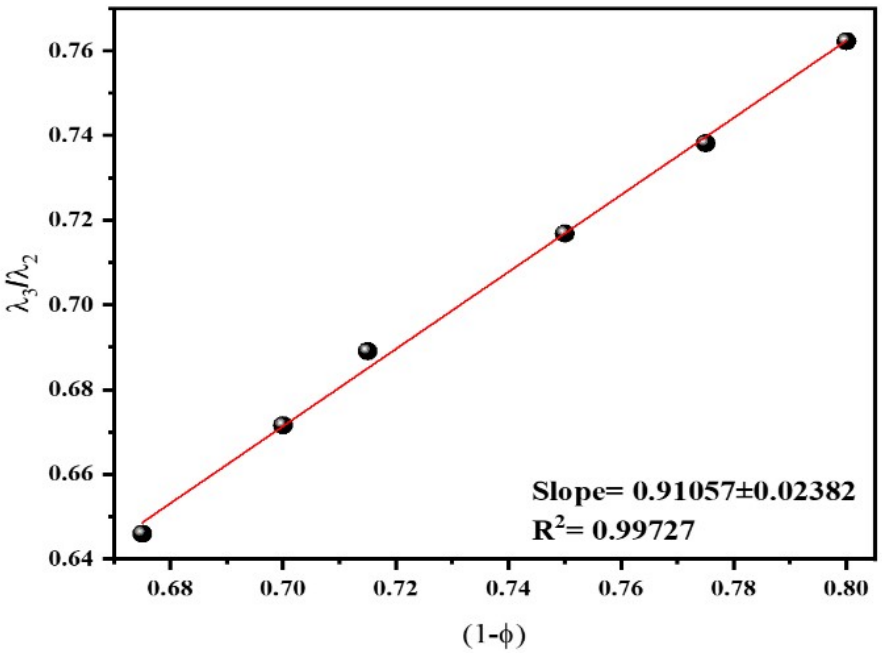

Figure S4: A graph illustrating the relationship between the wavelength ratio (λ_3/λ_2) and the weight fraction of the nonreactive mesogen $(1-\phi)$.

Figure S4 depicted the relationship between the wavelength of the photonic bandgap ratio (λ_3/λ_2) and the weight fraction of the nonreactive mesogen $(1-\phi)$. The increase in the refractive index (n_3/n_2) resulting from the extraction of the nonreactive mesogen in the LC-state was effectively represented by Equation (S3). The graph illustrated a notable trend wherein λ_3 decreased with increasing values of ϕ. This behavior could be attributed to the comparatively lower refractive index of 5CB compared to the other mesogens within the mixture. As a result, when a greater quantity of 5CB was extracted, the average refractive index of the remaining mixture decreased, leading to a reduction in the photonic bandgap wavelength. Moreover, the graph illustrated a linear correlation between the ratio of λ_3/λ_2 and $(1-\phi)$, indicating the impact of volume alteration resulting from the removal of the nonreactive mesogen and a corresponding reduction in pitch relative to the quantity of nonreactive mesogen removed. The significance of this graph resided in its practical utility for designing CLC mixtures with precise photonic bandgap wavelengths. To illustrate, if one had aspired to achieve a photonic bandgap wavelength of 500 nm, the graph served as a practical instrument for determining the requisite weight fraction of 5CB that needed to be extracted from the mixture in order to attain this specific wavelength.

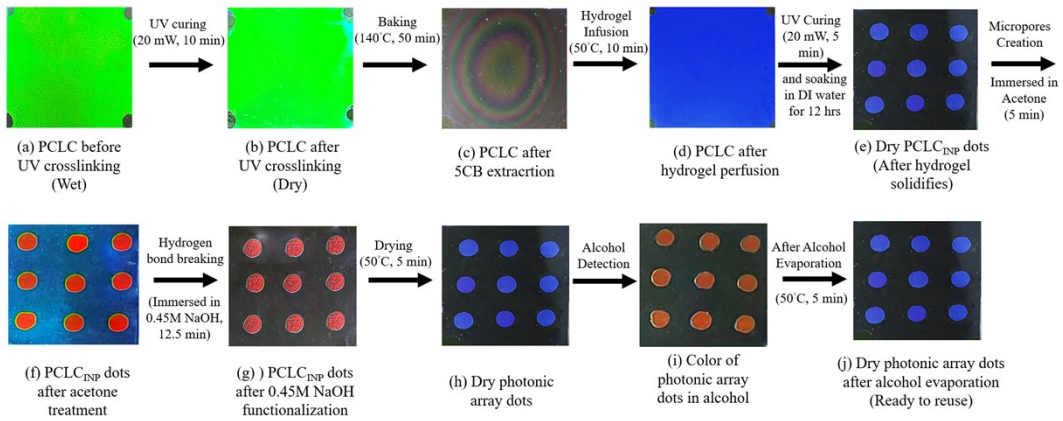

Figure S5: A step-by-step photographic sequence demonstrating the color transformation of a PCLC film throughout the sensor fabrication process, along with its subsequent use in alcohol detection.

Figure S6 illustrates the spectral response corresponding to various ethanol

concentrations, namely 5% (Fig. S6(a)), 10% (Fig. S6(b)), 30% (Fig. S6(c)), 40% (Fig. S6(d)), 60% (Fig. S6(e)), and 80% (Fig. S6(f)). In the case of 5% ethanol, the initial transmission band undergoes a shift from 451 nm at 0 seconds to 613 nm in just 1 second. Similarly, for 10% ethanol, the shift occurs from 452 nm at 0 seconds to 606 nm in 1 second. With a solution containing 30% ethanol, the shift is observed from 451 nm at 0 seconds to 586 nm in 1 second. Furthermore, for 40% ethanol, the initial transmission band shifts from 451 nm at 0 seconds to 563 nm in just 1 second. In the case of 60% ethanol, the initial transmission band undergoes a shift from 451 nm at 0 seconds to 548 nm in just 1 second. Notably, for a high concentration of 80% ethanol, the shift is minimal, moving only from 450 nm at 0 seconds to 470 nm in 1 second. This trend underscores that as the ethanol concentration increases, the extent of the wavelength shift diminishes, indicating a nonlinear relationship between the ethanol concentration and the observed shift in the transmission band. The experimental results reveal a rapid shift in the wavelength of the $PCLC_{IPN}$ dot's transmission spectrum, transitioning from green to red in just 10 seconds upon the introduction of an ethanol solution. This shift creates a broader transmission band compared to the original. The peak wavelength continues to redshift over time due to the absorption of ethanol molecules by carboxylic salt groups, leading to polymer network expansion and a widening of the transmission band. The maximum redshift occurs around 10 seconds, with minimal change in response to alcohol concentrations between 5% and 60%. However, for ethanol concentrations exceeding 60%, the redshift continues at a slower rate for up to 60 seconds. Figure S6(g) shows a time-dependent analysis of the wavelength shift of the $PCLC_{IPN}$ dot in response to different ethanol concentrations. The experimental results showed a rapid increase in wavelength shift over time, and highest at a specific time point. These observations collectively underscored the remarkable sensitivity and responsiveness of $PCLC_{IPN}$ dots to changes in ethanol concentration, exhibiting a rapid and visible response and rendering them highly effective for methanol concentration detection applications. In Figure S6(h), the monitored photonic wavelength bandgap (λ_{PBG}) values of the $PCLC_{IPN}$ array dot were presented throughout a sequence of 50 cycles. These observations involved alternating treatments with a 15 µL volume of a 40% ethanol solution, with each cycle initiating at both 0 seconds and 10 seconds. A noticeable color transition was observed during the repeated testing and evaporation cycles, shifting from red (with $\lambda_{PBG} \sim 640$ nm) to green (with $\lambda_{PBG} \sim 450$ nm). This significant color alternation signified that the developed

$PCLC_{IPN}$ array dot maintained repeatability throughout the entire experimental process, including the last cycle. It is noteworthy that this repeatability suggested the stability of the PCLCIPN array dot and its capacity for extended usage without any discernible loss in sensing capabilities. In conclusion, the developed $PCLC_{IPN}$ array dot demonstrated the requisite stability for repeated and prolonged usage, affirming its suitability for various sensing applications without compromising performance.

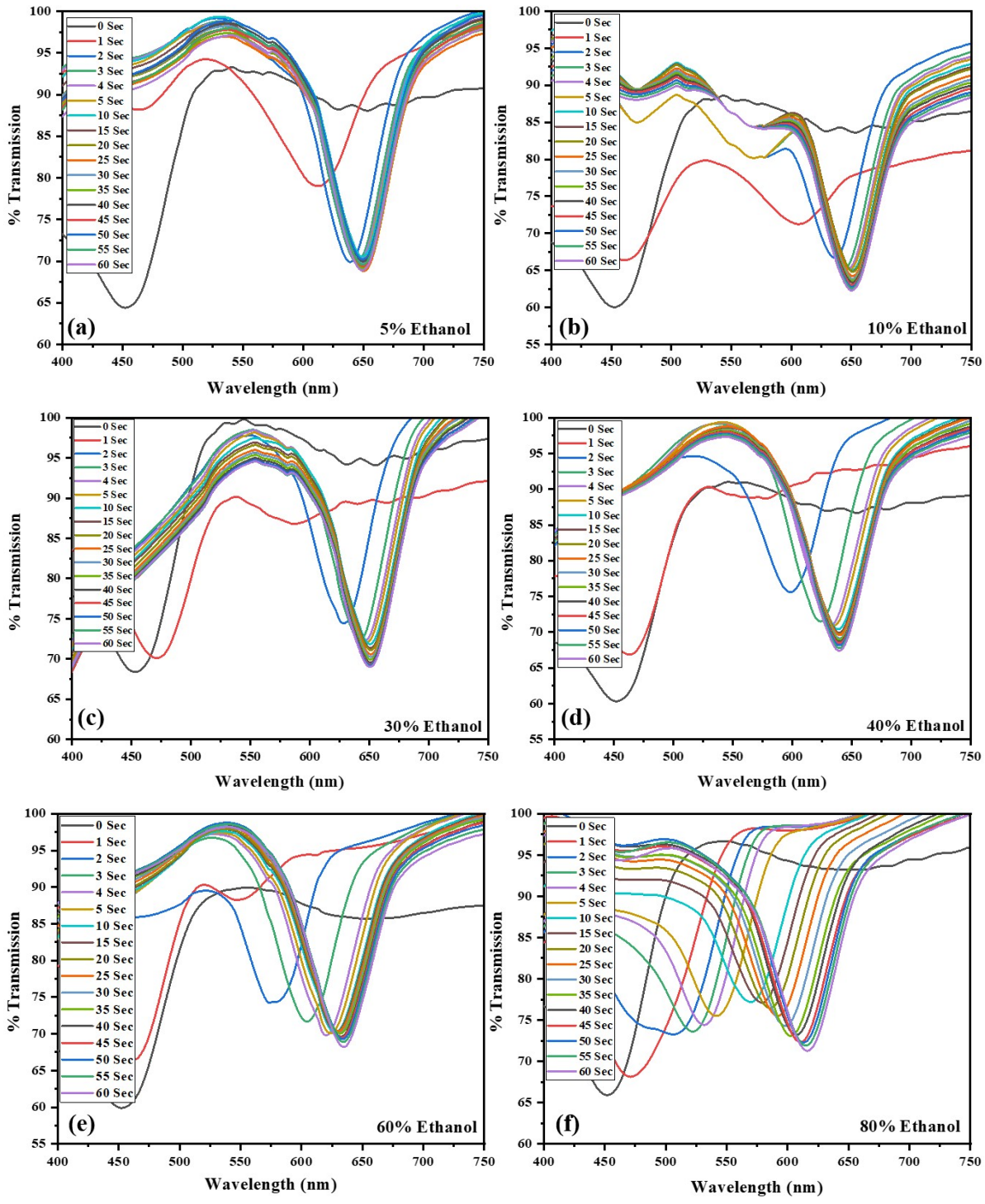

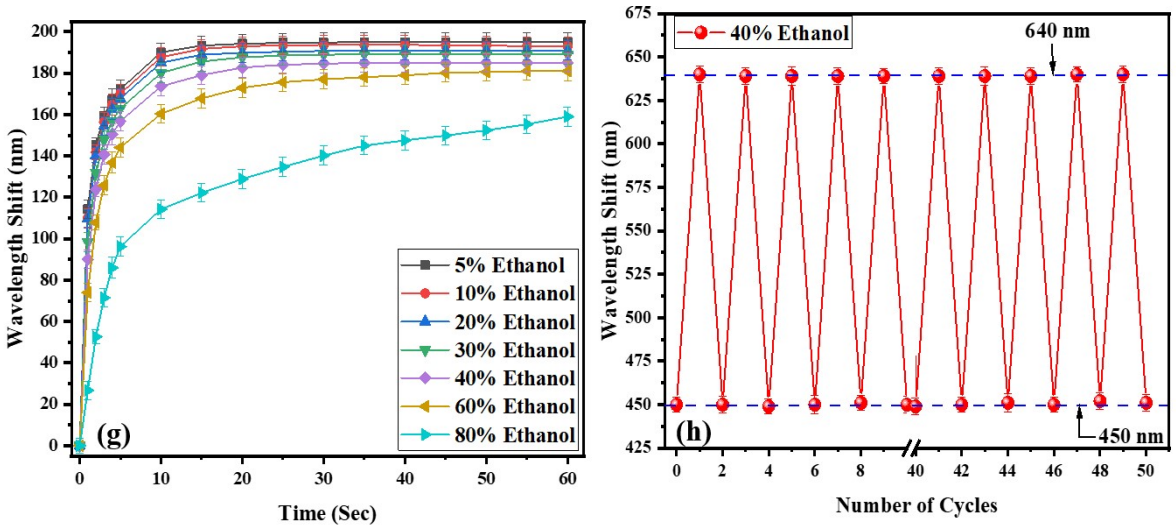

Figure S6: Time-lapse transmittance spectra are shown for the central dot within the $PCLC_{IPN}$ array dot when subjected to (a) 5% ethanol, (b) 10% ethanol, (c) 30% ethanol, (d) 40% ethanol, (e) 60% ethanol, (f) 80% ethanol, (g) time-dependent wavelength shifts of $PCLC_{IPN}$ dot upon exposure to solutions with different ethanol concentrations, and (h) the photonic wavelength bandgap (λ_{PBG}) values of the $PCLC_{IPN}$ array dot were monitored over a series of cycles, total 50 cycles. These cycles involved alternating treatments with a 15µL volume of a 40% ethanol solution at 0 second and 10 seconds.

Figure S7 depicted the time-lapse transmittance spectra observed during methanol detection. A 15µL methanol solution was applied to the central dot of the IPN array to monitor the change in the transmission band. The transmission band for the 5% methanol solution commenced at 468 nm at t = 0 seconds, rapidly transitioning to 601 nm within 1 second. Subsequently, the transmission band shift reached a state of saturation after approximately 10 seconds, stabilizing around ~632 nm (Fig. S7(a)). The initial transmission band for the 10% methanol solution appeared at 468 nm at 0 sec, rapidly transitioning to 562 nm within 1 second and saturated around ~630 nm at 10 sec (Fig. S7(b)). Similarly, for 30%, 40%, 60%, and 80% methanol solutions, a similar trend was observed. The initial transmission band was observed at ~468 nm, and it redshifted to 554 nm, 550 nm, 545 nm, and 524 nm, respectively (Fig. S7(c)-(f)). Notably, the transmission band shift in the methanol is lower than the ethanol due to attributed to the Hansen solubility parameter (HSP) as discussed in the main text.

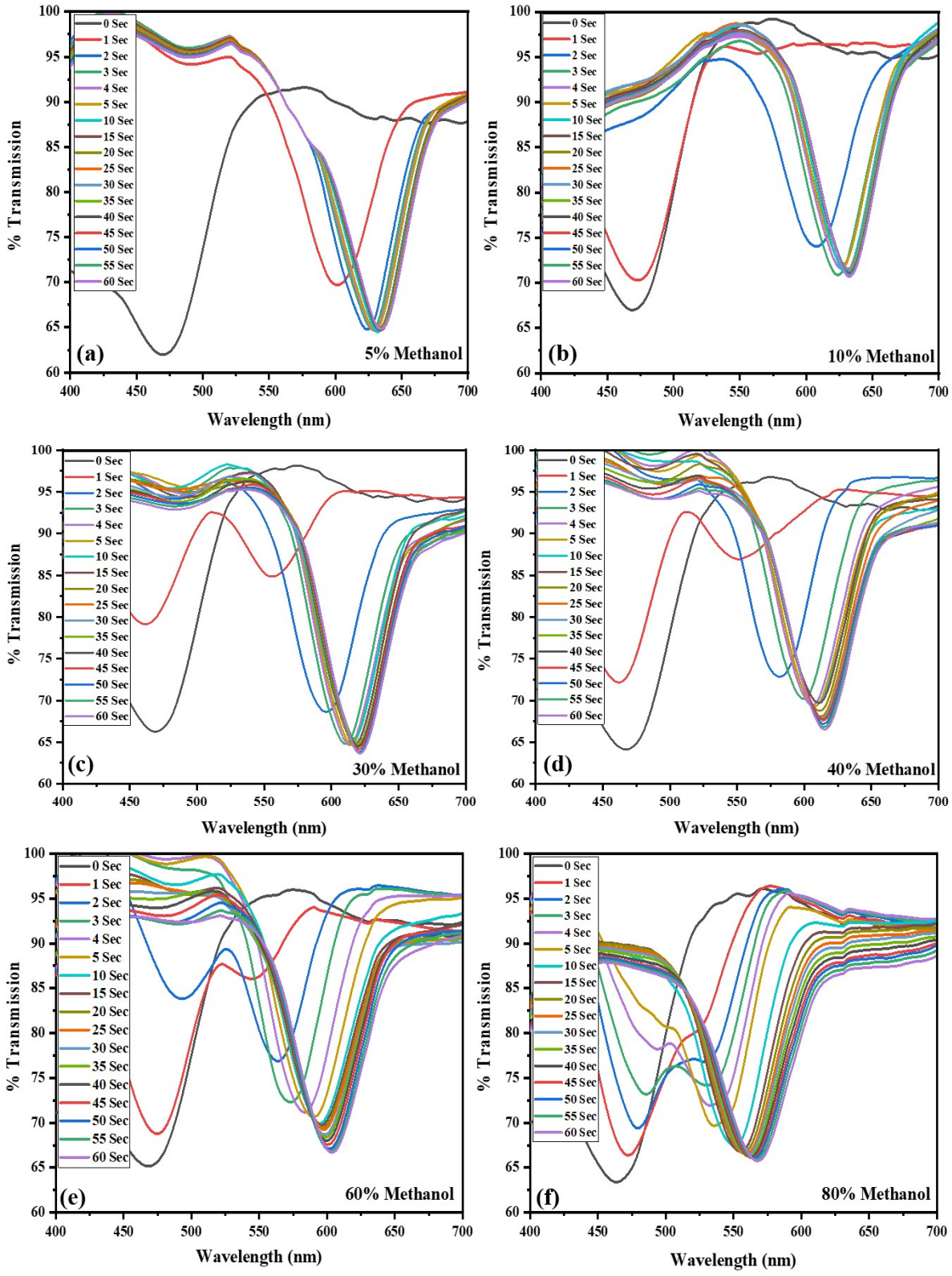

Figure S7: Time-lapse transmittance spectra are shown for the central dot within the $PCLC_{IPN}$ array dot when subjected to (a) 5% methanol, (b) 10% methanol, (c) 30% methanol, (d) 40% methanol, (e) 60% methanol, and (f) 80% methanol solutions.

- **Limit of Detection (LoD)**

The Limit of Detection (LoD) is defined as the minimum concentration of an analyte in a sample that is detectable, although not necessarily quantifiable, within the specified conditions of the test. [2] In the realm of a linear calibration curve, it is postulated that the instrument response (y) demonstrates a linear correlation with the standard concentration (x) within a defined concentration range. This correlation is established through the utilization of the linear regression method. [2]

$$y = ax + b \qquad \text{(S4)}$$

This model serves the purpose of calculating the sensitivity (b), as well as determining the LoD. Consequently, the expressions for LoD can be formulated as follows:[2, 3]

$$LoD = 3\frac{S_\alpha}{\beta} \qquad \text{(S5)}$$

where $S_\alpha = \sqrt{\frac{RSS}{DOF}}$ (S6)

Here S_α signifies the standard deviation of the response, while β denotes the slope of the calibration curve. The standard deviation of the response, S_α, can be estimated by examining either the standard deviation of y-residuals or y-intercepts of regression lines. The interpretation of standard deviation involves the utilization of the residual sum of squares (RSS) and degree of freedom (DoF). This methodology is universally applicable and particularly advantageous when the analytical method excludes background noise. It employs a calibration curve with a range of low values in close proximity to zero, and a more uniformly distributed set of values enhances the precision of the assessment.

Table S2: Calculated values of residual sum of squares (RSS), Slope (β), Degree of Freedom (DoF) and Limit of Detection (LoD)

Samples	RSS	Slope (β)	DoF	S_α	LoD
Ethanol	0.297167	0.43853	5	0.24378	1.66771
E: M::3:1	0.25061	0.44268	3	0.28903	1.95873
E:M::1:1	0.08782	0.49292	5	0.13253	0.80660

E:M::1:3	0.31098	0.53293	3	0.32196	1.81239
Methanol	0.46671	0.68527	5	0.30189	1.32162

➢ **Response and Recovery Time:**

The response and recovery times of our photonic alcohol sensor were measured as follows: The response time is approximately 10 seconds, as indicated by the saturation of the shift in the transmission band after this duration. The recovery time is 20 seconds, achieved by placing the sensor on a hotplate set to 40°C to evaporate any remaining alcohol in the $PCLC_{IPN}$ array dot post-detection. Subsequently, the alcohol solution on the IPN array dot was wiped away using a microfiber tissue paper.

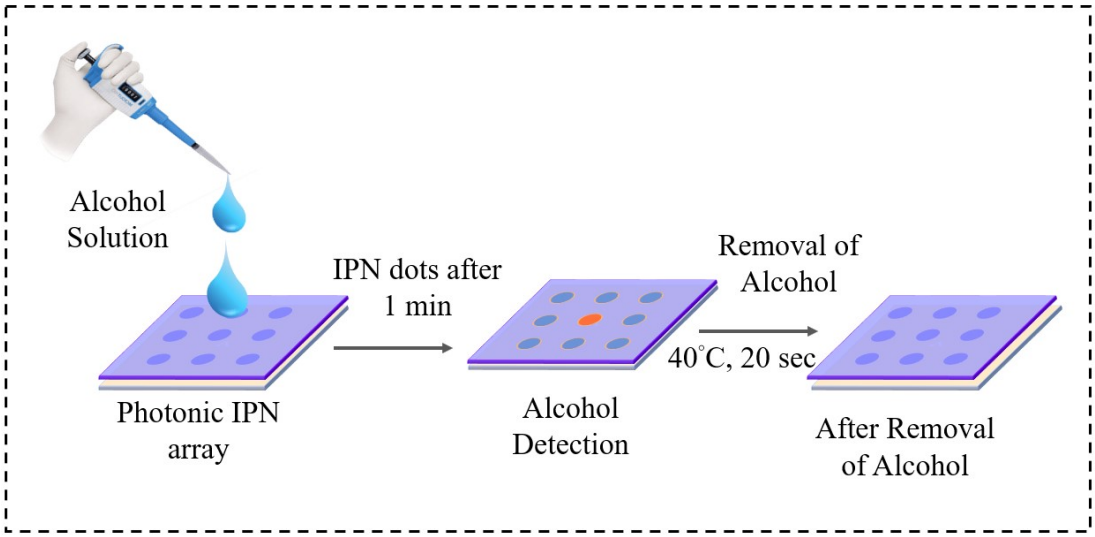

Figure S8: Response and recovery time measurement mechanism.

References:

1. K. Noh and S. Park, *Materials Horizons*, 2017, **4**, 633-640.
2. A. Procedures, *Food and Drug Administration, Center for Drug Evaluation and Research*, 2000.
3. P. Mishra, S. Navariya, P. Gupta, B. P. Singh, S. Chopra, S. Shrivastava and V. V. Agrawal, *Royal Society Open Science*, 2024, **11**, 231168.